Nuclear Instruments and Methods in Physics Research B 266 (2008) 4980–4986

Contents lists available at ScienceDirect

Nuclear Instruments and Methods in Physics Research B

journal homepage: www.elsevier.com/locate/nimb

ECR plasma assisted deposition of zinc nanowires

Vishwas S. Purohit, Shirshendu Dey, Somesh Kr. Bhattacharya, Anjali Kshirsagar, C.V. Dharmadhikari, S.V. Bhoraskar *

Department of Physics, University of Pune, Ganeshkhind, Pune 411 007, Maharashtra, India

ARTICLE INFO

Article history:
Received 9 January 2008
Received in revised form 13 August 2008
Available online 19 September 2008

PACS:
52.40−w
81.07.Bc
62.23.Hj
07.79.Cz

Keywords:
1-D nanowires
Nanoparticles
Zinc
Zinc hydride
ECR plasma

ABSTRACT

Deposits of one dimensional nanowires of zinc with diameters of 90–120 nm have been obtained by means of dc sputtering within an electron cyclotron resonance plasma reactor. The sputtering has been made effective by using a negatively biased cylindrical target. The structure of the nanocrystalline wires deposited on glass substrates were investigated with scanning electron microscopy, transmission electron microscopy and scanning tunneling microscopy. STM revealed that the structure of the one dimensional nanowires are ensemble of nanoclusters and nanowires with diameter of 4–5 nm. The crystalline nature of the metallic nanowires was studied with X-ray and electron diffraction analysis. The native oxide present on the metallic wires was revealed by photoluminescent spectroscopy. Theoretical modeling has been used to explain the possible mechanisms operative inside the plasma which lead into deposition of zinc on the substrate starting from the precursor species.

1. Introduction

Motivated by the fascinating electrical, catalytic and optical properties of the one dimensional metal nanostructures [1,2], many methods have evolved to synthesize these materials. Zinc is one of the most interesting materials for the fundamental research such as self assembled nanodomains and thermoelectric and magneto-resistance properties in nanowires [3–5]. One dimensional structures of zinc have been synthesized in number of ways [6] which include evaporation of ZnO powder mixed with graphite in an NH3 flowing carrying gas environment [7], the reaction of milled ZnO powder with ammonia [8,9], by evaporation of Zn grains in low vacuum at 200 °C [10] and by using vapor transport process on a zinc foil [11]. Here, we report for the first time, the use of microwave assisted plasma for depositing nanocrystalline zinc wires. Although applications of low pressure plasma devices for depositing varieties of thin films by chemical vapor deposition is well documented, there are few reports in the field of Electron Cyclotron Resonance (ECR) plasmas for depositing nanoparticles and one dimensional structures. [12–14] apart from extensive reviews for plasma based deposition by Ostrikov and Murphy [15,16] and other depositions [17–19]. Microwave assisted ECR low pressure plasmas are popularly used for depositing and processing of thin films and surfaces [20,21].

In the present paper, nanowires of zinc were deposited on glass substrates by the technique of chemical sputtering. The target material consisted of a cylindrical zinc metal sheet placed within a hydrogen plasma generated by the ECR plasma reactor. Unlike physical sputtering, in chemical sputtering, the ions of the plasma react chemically with the target material and the compound thus formed evaporates out through one of the several possible mechanisms. Hydrogen, due to its small mass, will not contribute meaningfully in the process of physical sputtering [22], however, it is observed to contribute towards the chemical sputtering. The high electron temperature ~15 eV and relatively confined geometry around the substrate is responsible for the high deposition rate of zinc atoms leading into nanostructures even in absence of catalyst.

The deposits were characterized by the techniques of transmission electron microscopy (TEM), scanning electron microscopy (SEM) and scanning tunneling microscopy (STM) for understanding the structure and morphology. The paper reports a new approach for synthesis involving confined sputtering for producing one dimensional crystalline zinc nanowires by making use of an ECR plasma, which has been modified to have a controlled growth of nanowires.

* Corresponding author. Tel.: +91 20 25692678x305; fax: +91 20 25691684.
E-mail address: svb@physics.unipune.ernet.in (S.V. Bhoraskar).

0168-583X/$ - see front matter © 2008 Elsevier B.V. All rights reserved.
doi:10.1016/j.nimb.2008.08.016

2. Experimental details

The plasma was excited by introducing hydrogen as a carrier gas into the ECR reactor chamber. The schematic of the experimental setup is shown in Fig. 1(a). The ECR plasma was excited by 2.45 GHz microwave source in TE11 mode inside a resonance cavity along with the required magnetic field of 875 Gauss generated by electromagnets. The ECR cavity consisted of a cylindrical stainless steel chamber, 15 cm in height and 12.5 cm in diameter and was coupled to the reactor chamber having a height of 30 cm and diameter of 20 cm. The reactor chamber contained various ports for introducing gases and other electrical feedthroughs. The 500 W microwave source was coupled through a quartz window to the resonance cavity. Base pressure was 10^{-5} mbar and operating pressure was 10^{-2} mbar.

A hollow cylinder of zinc metal, which served as the sputtering target, was mounted horizontally inside the processing chamber at a distance of 20 cm from the ECR zone. The cylinder was 12 mm in diameter and 30 mm in length. Its axis was kept transverse to the main reactor axis. Rectangular glass pieces of dimension 25×10 mm^2, were placed inside the cylinder as substrates for deposition. The substrates were cleaned by a standard wet

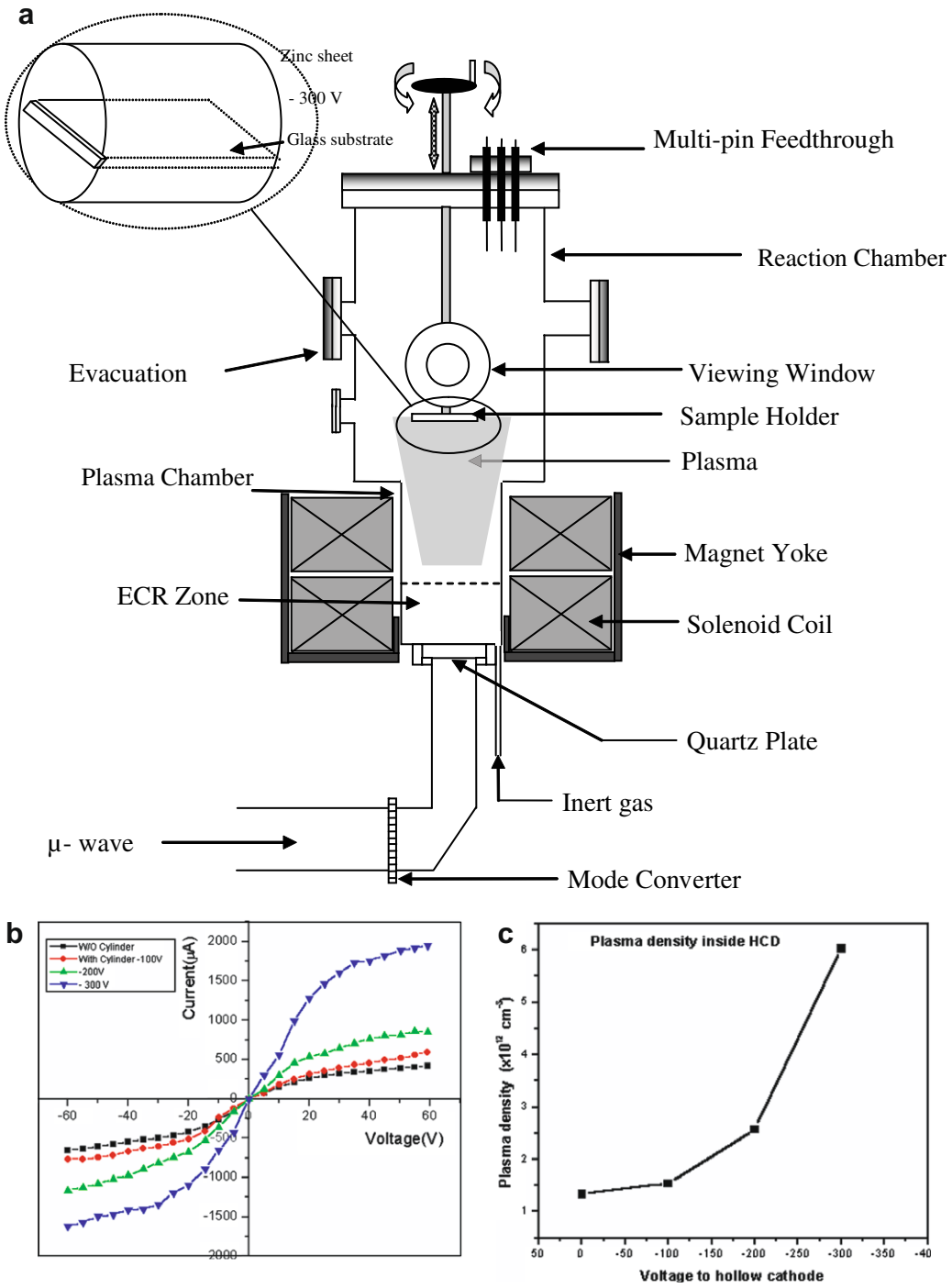

Fig. 1. (a) Schematic diagram of the hollow cathode sputtering assembly mounted inside the ECR plasma reactor at a distance of 20 cm from the ECR zone. (b) The *I–V* characteristic for hydrogen plasma by double probe method. (c) Graph of plasma density versus cathodic bias voltage.

cleaning process including ultrasonication before inserting into the hollow cylinder. A negative bias voltage of 300 V was applied to the target cylinder with reference to the chamber which was kept at the ground potential. The deposition time was 30 min.

The intensity of the hydrogen plasma inside the cylindrical sputterer was seen to be higher than that compared to the surroundings as evident from the increase in glow. The plasma density was estimated from the Langmuir double probe measurements carried out by keeping the probes inside the negatively biased cathode. Plasma density was calculated from the *I–V* characteristics following the standard procedure used in Langmuir double probe technique [23]. The electron density estimated from the probe currents, is plotted as a function of the negative bias voltage on the cylindrical cathode and is seen in Fig. 1(b). The plasma density is seen to increase with increasing voltage and is around six times higher at 300 V compared to the one obtained at no bias as shown in Fig. 1(c). The electron temperature was estimated to be around 15 eV.

Scanning electron microscope [JEOL-JSM-6360A] was used to reveal the physical structure of the samples. STM and TEM analysis were used for much closer investigation of the growth morphology. TEM micrographs were recorded for the nanocrystalline powder, scrapped out from the substrate, supported by carbon-coated grids. A home-built scanning tunneling microscope based on a fine mechanical-screw-lever arrangement assembly with a compact four-quadrant three-dimensional scanner was used for STM investigation [24]. One of the most widely used test samples for STM is highly oriented pyrolytic graphite (HOPG) because of its reasonable flatness in the sub-nanometer range and non-reacting nature. The sample for STM analysis was prepared by putting a very dilute drop of the nanowire solution on the HOPG substrate followed by subsequent drying for 5 min. STM studies were carried out immediately after the deposition. The STM tips were made from 0.025 cm diameter polycrystalline Pt–Rh wires by mechanical cutting, at an angle. Details of the system and the general procedure for imaging are discussed elsewhere [25]. The images were processed using SPIP software [26]. XRD and photoluminescence studies were also carried out.

3. Results and discussion

The film deposited on the glass substrates placed inside the hollow cylindrical cathode assembly, was seen to be weakly adhesive to the substrate. The crystal structure and the crystalline phases were studied by scrapping off the deposits. Scanning electron micrographs, recorded for the deposited nanowires are presented in Fig. 2(a). The observed nanowires are 90–120 nm in diameter with average length of 10–20 μm. The XRD pattern is shown in Fig. 2(b) and is compared with the ASTM data for crystalline zinc.

Fig. 2(c) exhibits the transmission electron micrograph and Fig. 2(d) shows the Selective Area Diffraction (SAD) pattern. TEM observation revealed that each nanowire consisted of smaller stubby growth at the periphery. The diameters of the nanowires are, on an average seen to vary between 100 and 120 nm with length between 5 and 6 μm. Large number of Y joints are also seen. The interplanar separations were calculated from the SAD pattern for a single nanowire (observed under TEM) and it is found that the nanowire consisted of zinc and zinc oxide. The indices for metallic zinc include (100), (101), (002), (102) and (103). The plane (400) corresponds to zinc oxide. Thin oxide layer must have been grown on the zinc wire after exposure to atmosphere which could be detected by TEM but not from the X-ray diffraction pattern.

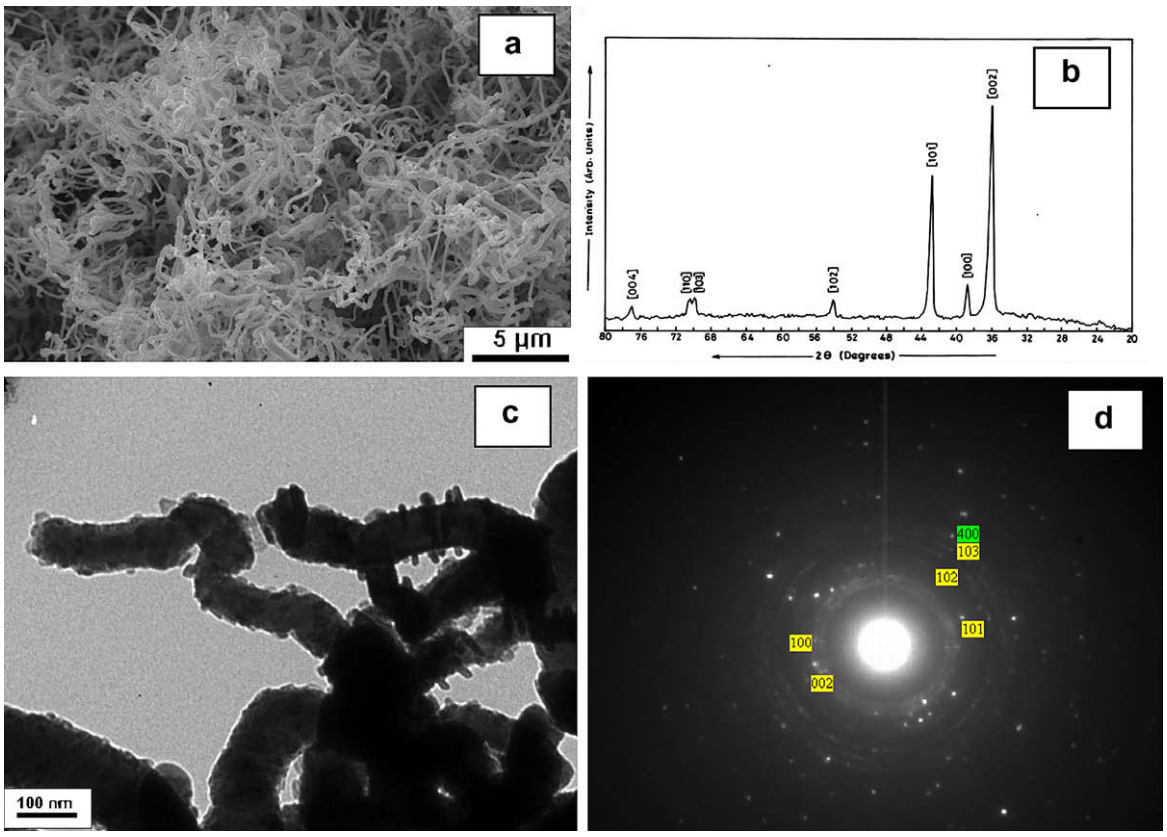

Fig. 2. (a) SEM micrographs of sputter deposited zinc for 30 min. (b) X-ray diffraction pattern for the as prepared sample. (c) Transmission Electron Micrographs of the zinc nanowires. (d) SAD Pattern for a single nanowire.

The deposits were further characterized using scanning tunneling microscope with an optimum value of tunnel current of 0.1 nA and a bias voltage of 84 mV in constant current mode. The time between the imaging and the sample preparation was kept to a minimum of 5 min. It was found that once the wires are located, with some difficulty they could be imaged repeatedly.

Fig. 3(a) shows an image with a scan-area of 1000 nm × 1000 nm. The nanowires are seen to be more than 1 μm in length and 120 nm in diameter as seen from the corresponding line scan shown in Fig. 3(b). These results are in good agreement with the value of around 120 nm obtained from TEM studies. Closer observations at higher magnifications reveal very interesting information about the morphology of the nanowires. Imaging at predetermined small area of 100 nm × 100 nm is shown in Fig. 3(c), which revealed the presence of nanoparticles as well as nanowires. It seems that the surface of the larger nanowires or nanoassembly are composed of still smaller nanowires having sizes 5–7 nm and nanoparticles of size 5 nm. The line scan of the smaller nanowires is seen in Fig. 3(d) and it confirms the observations.

The present method of growing crystalline Zn nanowires is, no doubt, a physical method where no attempt is made to passivate the metallic wires from oxidation when exposed to atmosphere. As an effect, unintentional growth of oxide layer is expected to occur on the surface of these nanowires. The oxide layer seems to be too thin to be observed in the X-ray diffraction pattern. However, the presence of this is observed in the selective area diffraction pattern during the TEM analysis. In order to ascertain the presence of the oxide layer we tried to detect the optical property of the surface since ZnO is a luminescent material on account of high concentrations of defect sites at surface regions of nanomaterials present in the structure. Room temperature luminescence is reported to occur around 400 nm in case of nanocrystalline ZnO [27,28]. Fig. 4 represents the photoluminescence spectrum of the nanowires of Zn grown in the present experiments .A single broad peak, centered at 408 nm, thus ascertains the presence of oxide species covered on the surface of the Zn nanowires. Presence of thin ZnO layer is confirmed in the selective area diffraction analysis also.

The observed behavior of the deposit in the present experiments leading to the formation of nanostructures is interesting. Since such kind of product is not usually produced in the ECR plasma, the presence of negatively biased cylindrical sputtering target seems to be providing some unique characteristics.

In the present ECR reactor the electrons present in the plasma, particularly those inside the cylindrical target, are accelerated towards the axial glow region as depicted in Fig. 5. Subsequently, hydrogen ions get accelerated towards the cathode to chemically sputter out the zinc atoms. As is known, conventional sputtering is usually carried out with inert gases such as argon, wherein the ionized atoms are accelerated towards the target. This process transfers the high momentum of the ions to the target atoms and locally energized atoms evaporate into the plasma and are then

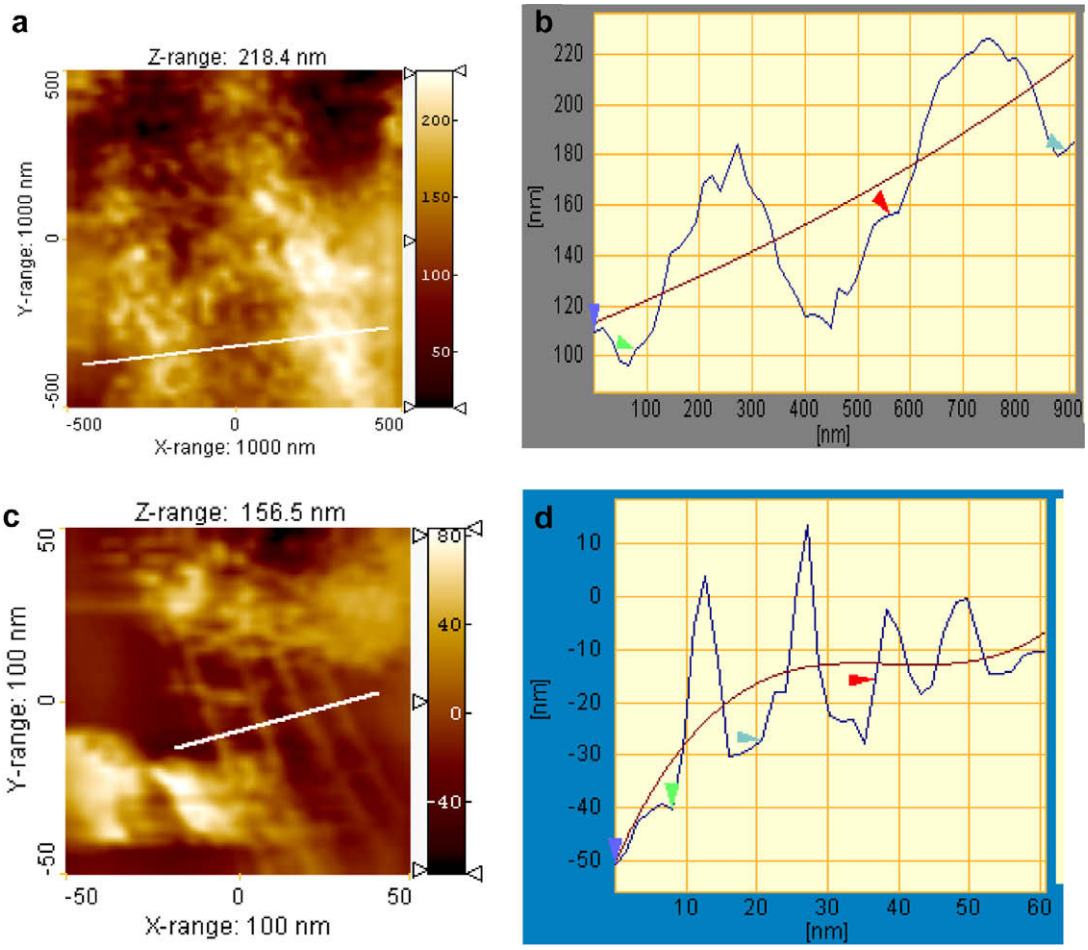

Fig. 3. STM images of zinc nanowire. (a) Image recorded at lower magnification with constant current mode for a scan-area of 1000 nm × 1000 nm. The parameters were I_t = 0.06 nA and V_{bias} = 80 mV; White lines indicates the direction along with the Z profile plot is recorded and is exhibited in part b. (b) Z profile plot corresponding to (a). (c) Image recorded at higher magnification for a scan-area of 100 nm × 100 nm. White lines indicates the direction along with the Z profile plot is recorded and is exhibited in part d. (d) Z profile plot corresponding to (C).

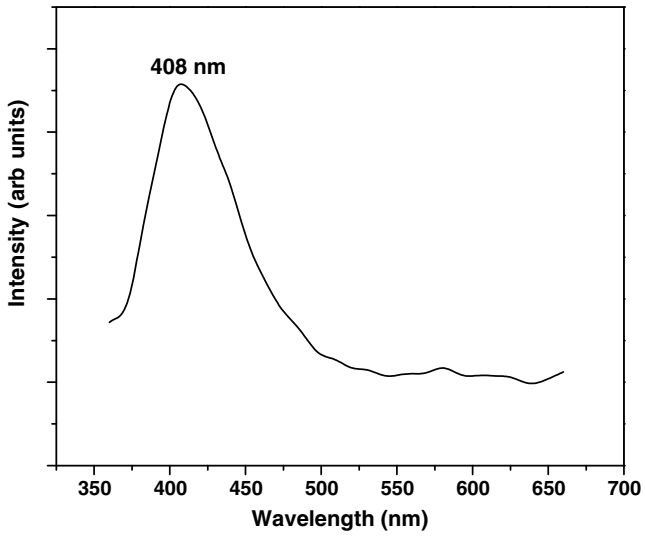

Fig. 4. Room temperature photo luminescence spectrum of the as prepared zinc nanowires dispersed in methanol.

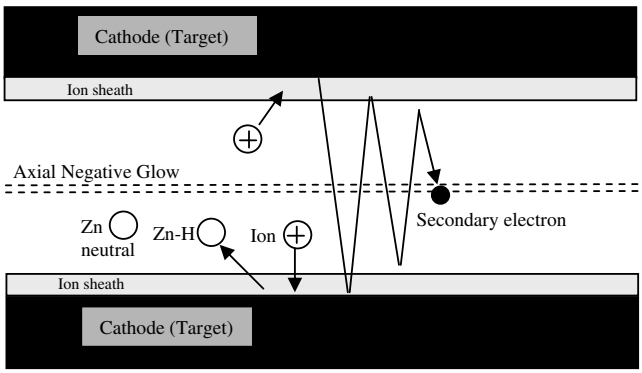

Fig. 5. Schematic diagram explaining the sputtering process inside the cylindrical sputterer.

deposited onto the substrate. However, when hydrogen is used as the ionizing gas, the conventional physical approach to sputtering is not valid. This is because the mass of the hydrogen ion is comparatively much smaller than the target atom mass. Hydrogen, particularly atomic hydrogen, chemically reacts with zinc to form zinc

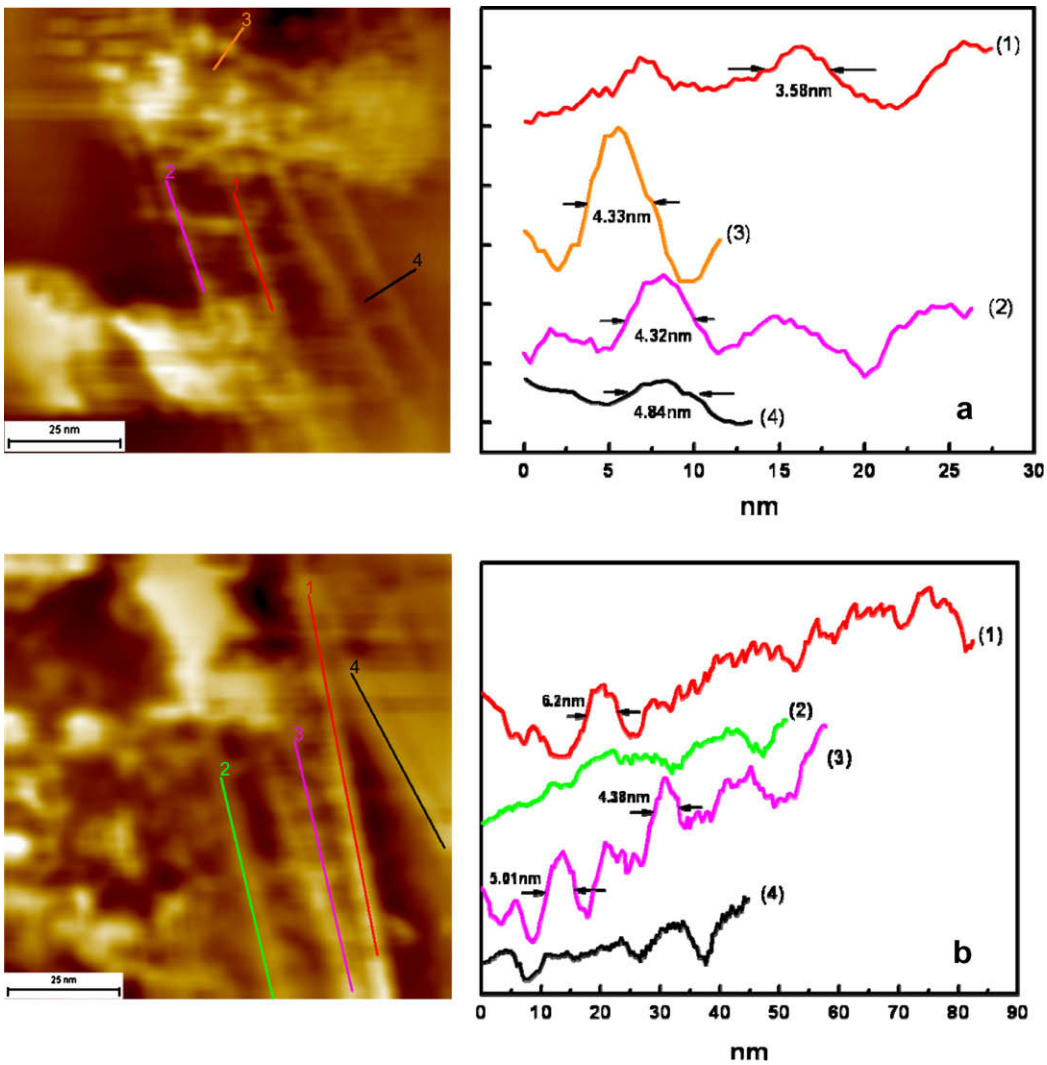

Fig. 6. STM scans on nanowires. (a) Scan shows linear arrangement of particles having cluster sizes around 4.2 nm. (b) Different scan-area shows particles around 4.5 nm to assemble linearly.

hydride (ZnH_2) [29]. Since the electron temperature in the hydrogen rich ECR plasma is measured to be around 15 eV, at the operating pressure in the present experiments, it is quite possible that as a result of the interaction with the precursors, various other species of zinc hydride like ZnH or ZnH^+ may also be formed.

In the present case, these hydride species are expected to act as the precursors for the growth of zinc nanoclusters onto the glass substrate. Subsequent motion of the hydride precursors, towards the negatively charged glass substrate, is then expected. The positively charged hydride precursor may capture an electron and release energy, sufficient to assist its dissociation, leading into the metal atom. As a result, heterogeneous nucleation occurs on the substrate with the evolution of hydrogen molecules. Alternatively, ZnH species can also dissociate into Zn and H inside the plasma, near the substrate. However the actual phenomena, involved in the growth process, may be more complex than what is assumed.

In order to verify the above proposed mechanism, we have performed ab-initio calculation for ZnH_2, ZnH and ZnH^+ molecules using the Vienna ab-initio Simulation Package (VASP) [30]. The geometries of the molecules were optimized using conjugate gradient method [31]. We use Perdew–Burke–Ernzerhof (PBE) exchange correlation [32] and plane augmented wave (PAW) method [33]. The valence electronic configuration for Zn and H are taken to be $3d^{10}4s^2$ and $1s^1$, respectively. The energy and force convergence were set to 10^{-4} eV and 10^{-3} eV/Å, respectively. ZnH_2 and ZnH are stable linear molecules having bond lengths of 1.54 Å and 1.63 Å, respectively. The binding energies are 2.18 eV/atom for ZnH_2 and 0.85 eV/atom for ZnH. On the other hand, ZnH^+ is found to be an unstable molecule with no bound state. The formation of ZnH^+ can be explained by the ionization energy and partial charge density of the highest occupied molecular orbital (HOMO) of ZnH whose ionization potential is 6.6 eV. When electrons with 15 eV energy collide with ZnH moiety, it strips away the an electron in s orbital resulting into the formation of ZnH^+. Since ZnH^+ is unstable, it dissociates into Zn atom and H^+ ion. The H^+ ion picks up an electron due to its high electron affinity and neutralizes to an H atom where as the Zn atoms agglomerate to give the resulting Zn cluster. The H atoms further form H_2 molecules.

Alternative to this we may also expect that ZnH_2 dissociates to give Zn and H. However, the mechanism involved is different from ZnH. Calculation of the fragmentation energies (Δ) for ZnH_2 is shown below:

$$ZnH_2 \rightarrow Zn + 2H \quad \text{with} \quad \Delta = 6.527\ \text{eV} \quad \text{where}$$
$$\Delta = E(Zn) + 2E(H) - E(ZnH_2).$$

Whereas,

$$ZnH_2 \rightarrow ZnH + H \quad \text{gives} \quad \Delta = 4.82\ \text{eV} \quad \text{where}$$
$$\Delta = E(ZnH) + E(H) - E(ZnH).$$

The Δ values for the above two pathways suggest that ZnH_2 will dissociate first into ZnH and H. The ZnH thus formed will then yield neutral Zn as mentioned above.

We also believe that the zinc clusters subsequently get self assembled to form the fibers. The dominant forces responsible for particle transport seem to be electrostatic, neutral drag as well as self diffusion. Moreover, the glass substrate itself may accumulate nonuniform negative charges on the surface on account of the regions of crystalline pockets surrounded by the amorphous structure. The high surface roughness as well as the low thermal conductivity of the substrate can cause differential crystal nucleations and varied growth process. The confined geometry in the cylindrical target supports the formation of nanowires without the presence of catalyst.

In fact, the line scan in the STM image of Fig. 6 shows the clusters of around 4 nm in diameter which are seen to get linearly arranged to form the fibers. The STM images also show that the fibers further get bundled together to grow into the nanowires of larger diameters.

Similar growth models are explained by Ostrikov [15]. It seems clear that in the beginning of the sputtering process, individual particles are grown at each nucleating site. After reaching a critical number density, zinc forms larger clusters on the glass surface forming nanofiber like assemblies.

4. Conclusions

In conclusion, the hydrogen ion assisted chemical sputtering in an ECR plasma is seen to produce nanowires of zinc on the glass substrate. The energetic electrons in the ECR plasma are responsible to dissociate the hydride precursors of zinc ejected from the metallic target. The paper throws light on the structural morphology zinc nanowires which was observed using the scanning tunneling microscopic techniques. The high-resolution STM images have also helped us in understanding the self assembly of zinc clusters (~4 nm) on glass substrates. Theoretical calculations support the dissociation of zinc hydride species into neutral zinc atoms. However, there seems to be complex phenomenon on account of the different kinds of charged and neutral species present in the plasma and only a speculative conclusion can be drawn about the deposition process.

Acknowledgement

The Department of Science and Technology is acknowledged for the financial support.

References

[1] Y.G. Sun, B. Gates, B. Mayers, Y.N. Xia, Nano Lett. 2 (2002) 165.
[2] Y.G. Sun, Y.N. Xia, Adv. Mater. 14 (2002) 833.
[3] Q. Li, K.W. Kwong, Phys. Rev. Lett. 92 (2004) 186102.
[4] J.P. Heremans, C.M. Thrush, D.T. Morelli, M.C. Wu, Phys. Rev. Lett. 91 (2003) 076804.
[5] Q. Li, C. Wang, Chem. Phys. Lett. 375 (2003) 525.
[6] Y.W. Wang, L.D. Zhang, G.W. Meng, C.H. Liang, G.Z. Wang, S.H. Sun, Chem. Commun. 24 (2001) 2632.
[7] Y.F. Yan, P. Liu, M.J. Romero, M.M. Al-Jassim, J. Appl. Phys. 93 (2003) 4807.
[8] J. Li, X.L. Chen, Solid State Commun. 131 (2004) 769.
[9] S.S. Chang, S.O. Yoon, H.J. Park, A. Sakai, Mater. Lett. 53 (2002) 432.
[10] J. Liu, Z. Zhang, X. Su, Ye. Zhao, J. Phys. D: Appl. Phys. 38 (2005) 1068.
[11] X. Wen, Y. Fang, S. Yang, Angew. Chem., Int. Ed. 44 (2005) 3562.
[12] C.M. Hsu, C.H. Lin, H.L. Chang, C.T. Kuo, Thin Solid Films 225 (2002) 420.
[13] X.W. Liu, J.H. Lin, W.J. Hsieh, H.C. Shih, Diam. Relat. Mater. 11 (2002) 1193.
[14] X.W. Liu, L.H. Chan, K.H. Hong, H.C. Shih, Thin Solid Films 212 (2002) 420.
[15] K. Ostrikov, Rev. Mod. Phys. 77 (2005) 489.
[16] K. Ostrikov, A.B. Murphy, J. Phys. D: Appl. Phys. 40 (2007) 2223.
[17] J. Shieh, C.H. Lin, M.C. Yang, J. Phys. D: Appl. Phys. 40 (2007) 2242.
[18] S.A. Barve et al., J. Phys.: Conf. Ser. 114 (2008) 012045. 7pp.
[19] K. Ostrikov, J.D. Long, P.P. Rutkevych, S. Xu, Vacuum 80 (2006) 1126.
[20] R.M.A.A. Majeed, V. Purohit, R. Bhide, A.B. Mandale, S.V. Bhoraskar, V.N. Bhoraskar, J. Phys. D: Appl. Phys. 39 (2006) 2109.
[21] R.M.A.A. Majeed, V.S. Purohit, S.V. Bhoraskar, A.B. Mandale, V.N. Bhoraskar, Radiat. Eff. Defect Solid 161 (2006) 495.
[22] C.V. Budtz-Jorgensen, P. Kringhoj, J.F. Nielsen, J. Bottigerm, Surf. Coat. Technol. 135 (2001) 299.
[23] A. Grill, Cold Plasma in Material Fabrication: From Fundamentals to Applications (ISBN 978-0-7803-4714-4), IEEE Press, 1994, p. 134.
[24] (a) W.J. Kaiser, R.C. Jaklevic, Surf. Science 1181 (1987) 55;
(b) G. Binning, D.P.E. Smith, Rev. Sci. Instr. 57 (1986) 1688;
(c) C.V. Dharmadhikari, in: R.A. Meyers (Ed.), Encyclopedia of Analytical Chemistry: Instrumentation and Applications, John Wiley, Chichester, UK, 2000, p. 9284.
[25] S. Datar, M. Kumar, M. Sastry, C.V. Dharmadhikari, Colloid Surf. A 232/1 (2004) 11.
[26] SPIP stands for Scanning Probe Image Processor, which is software for scanning probe microscopy and other microscopy techniques developed by Image Metrology, Denmark.
[27] Xiao-Jie Yang, Xin-Yu Miao, Xiao-Liang Xu, Chuan-Ming Xu, Jun Xu, Hong-Tu Liu, Opt. Mater. 27 (2005) 1602.
[28] D.H. Liu, L. Liao, J.C. Li, H.X. Guo, Q. Fu, Mater. Sci. Eng. B 121 (2005) 77.

[29] Alireza Shayesteh, Shanshan Yu, Peter F. Bernath, Chem. Eur. J. 11 (2005) 4709.
[30] (a) G. Kresse, J. Furthmuller, Phys. Rev. B 54 (1996) 11169;
(b) G. Kresse, J. Furthmuller, Comput. Mater. Sci. 6 (1996) 15.
[31] N. Kosugi, J. Comput. Phys. 55 (1984) 426.
[32] J.P. Perdew, K. Burke, M. Ernzerhof, Phys. Rev. Lett. 77 (1996) 3865.
[33] (a) P.E. Blochl, Phys. Rev. B 50 (1994) 17953;
(b) G. Kresse, J. Joubert, Phys. Rev. B 59 (1999) 1758.